Artificial magnetism and anticrossing interaction in photonic crystals and split-ring structures

Ruey-Lin Chern[1,*] and Didier Felbacq[2]
[1]*Institute of Applied Mechanics, National Taiwan University, Taipei 106, Taiwan, Republic of China*
[2]*GES UMR-CNRS 5650, Université de Montpellier II, Bâtiment 21, CC074, Place E. Bataillon, 34095 Montpellier Cedex 05, France*
(Received 30 October 2008; published 20 February 2009)

In this paper, the authors conduct a study of artificial magnetism and anticrossing interaction that arise in photonic crystals and split-ring structures. The magnetic activity comes from localization of fields in photonic crystals with large dielectric contrast as well as in split-ring structures with the defectlike resonance. Both structures exhibit similar dispersion features near the resonance, whose effective permeability can be described in terms of the Lorentz-type oscillators. In particular, strong magnetic response is accompanied with the anticrossing interaction between the two fundamental frequency branches. This feature is characterized by a simple dynamic model which incorporates the coupling between a free and a localized photon state and illustrated with the transition of mode patterns where the fields mutually exchange their localization nature as the wave number changes.

DOI: 10.1103/PhysRevB.79.075118 PACS number(s): 42.70.Qs, 41.20.Jb, 73.20.Mf, 78.20.Ci

I. INTRODUCTION

Artificial magnetism in an essentially nonmagnetic medium is one of the most distinguished features in metamaterials.[1–3] This unusual property comes from the *resonance* of fields inside the microstructures that compose the medium and becomes significant when the free-space wavelength is much larger than the microstructure size. Artificial magnetism is therefore *quasistatic* in nature, and along with it usually comes a *localized* field distribution within the microstructure. A very inhomogeneous field is required to produce a large magnetic activity,[1] and an *adverse* response is even possible once the frequency goes above the intrinsic resonance.[4,5] By regarding the structure as a homogeneous medium, the *effective* permeability can be negative over a certain frequency range, which corresponds to the forbidden gap in the dispersion diagram. This feature consists with the localized nature of artificial magnetism; the fields are largely confined within individual elements. Propagation of the electromagnetic fields in the medium is thus prohibited.

Metal rings were known to possess the diamagnetic property due to the conducting current loop associated with the ring geometry.[6] As a gap is introduced to build the split-ring configuration, the magnetic response will be enhanced due to the resonance. This type of resonance is analogous to that in the *LC* circuit, where the conduction currents are circulating around the ring element and resulting in a significant magnetic moment. An equivalent circuit model was proposed to depict the artificial magnetism and lead to an effective permeability under the long-wavelength assumption.[1] In another aspect, artificial magnetism occurs as well in photonic crystals with large dielectric contrast.[7] This is due to the concentration of fields within the high dielectric region, which produces intensive polarization currents circulating around the dielectric element. A theory of mesoscopic magnetism based on the multiscale expansions was appealed to describe the effective permeability in terms of a sum of Lorentz-type oscillators.[8] The respective oscillations are identified as the *waveguide* modes associated with the dielectric geometry. A negative value of the effective permeability is also possible when the frequency exceeds the embedded resonance. This feature confirms that a periodic structure mimics a metamaterial.[9] An analysis based on the complex band structure was recently presented for the interpretation of artificial magnetism for periodic metal-dielectric-metal layered structures.[10] The use of complex band structure establishes additional criteria for the validity of effective-medium description for metamaterials, where the attenuation of electromagnetic waves has been considered.

In this paper, the author investigates the important features of artificial magnetism and its related anticrossing behavior, with emphasis on the correspondences between photonic crystals and split-ring structures. The theory of mesoscopic magnetism in photonic crystals[8] is revisited and employed in split-ring structures with a slight modification. Two similar features related to artificial magnetism will be identified in both types of structures. First, the fields are strongly localized within individual elements with rather weak interactions between neighboring cells. Near the resonance, the magnetic fields are greatly enhanced inside the dielectrics or split rings, while outside the fields are substantially reduced. The split-ring structure shows a more efficient mechanism for concentration of fields and a larger and near-optimal resonance strength, where the intrinsic *LC* resonance corresponds to the lowest-order Lorentz-type oscillator. Second, in the frequency range where strong artificial magnetism occurs, the two fundamental branches exhibit an *anticrossing* interaction. There exists the *like symmetry* in the eigenmodes on the two branches, causing them to repel each other. The anticrossing behavior can be characterized by a simple dynamic model which incorporates the coupling coefficient between a free photon state and a localized photon state as the interaction strength. This feature is further illustrated with the transition of modes on the respective branches, where the fields mutually exchanged their localization nature as the wave number changes.

 ©2009 The American Physical Society

II. BASIC EQUATIONS

A. Dispersion characteristics

Dispersion is a property of wave that interacts with a medium. Important features are either manifest or implied in the dispersion characteristics. For periodic structures made of identical elements, dispersion features are embedded in the eigensystem based on the electromagnetic wave equation and the Bloch condition. The magnetic response for a two-dimensional array of dielectric or split-ring columns is described by the transverse electric (TE) modes, where the E field lies completely in the lattice plane as

$$-\nabla\left(\frac{1}{\varepsilon}\nabla H\right)=\left(\frac{\omega}{c}\right)^2 H, \tag{1}$$

where H is the magnetic field along the column axis. For a periodic lattice with infinite extent, it is sufficient to solve the underlying problem in one unit cell, along with the Bloch condition

$$H(\mathbf{r}+\mathbf{a}_i)=e^{i\mathbf{k}\cdot\mathbf{a}_i}H(\mathbf{r}) \tag{2}$$

applying at the unit-cell boundary, where $\mathbf{k}$ is the Bloch wave vector and $\mathbf{a}_i$ $(i=1,2)$ is the lattice translation vector. The eigensystem (1) which considers the frequency as unknown is to be solved by the inverse iteration method for dielectric structures[11,12] or the interface matching method for metal structures.[13–15] For pure dielectric structures, no special treatment is needed at the interface between different media, whereas it is indispensable for metal structures. By matching the boundary condition at the interface, important features pertaining to metals can be resolved in detail. This is particularly true when the plasmonic property increases its importance and the effect of skin depth on the dispersion characteristics becomes significant.

B. Artificial magnetism

Artificial magnetism arises in a structure where the magnetic fields are sufficiently localized. This was realized in a photonic crystal with large dielectric contrast.[7] For TE polarization, the H fields are largely confined in the high dielectric regions and the polarization currents are circulating around the dielectric element, giving rise to a significant magnetic moment. Let ε_d be the dielectric constant of the cylinder and the background material is assumed to be air. Based on the theory of mesoscopic magnetism,[8,16,17] the effective permeability is expressed as a sum of Lorentz-type oscillators

$$\mu_{\text{eff}}=1+f\sum_n \frac{\beta_n\omega^2}{\omega_n^2-\omega^2},\quad \beta_n=\frac{\langle\psi_n,1\rangle^2}{\langle\psi_n,\psi_n\rangle\langle 1,1\rangle}, \tag{3}$$

where f is the fraction of dielectric material, ω_n and ψ_n are the nth solution pair of the eigensystem $-\nabla^2\psi=\varepsilon_d(\omega/c)^2\psi$, defined at the *interior* of high dielectric region Ω with $\psi=0$ on its boundary, and the inner product $\langle f,g\rangle\equiv\int_\Omega f^* g d\tau$ is an integral taken over the region Ω. In Eq. (3), β_n is considered the *strength* of nth-order resonance, and ψ_n is the corresponding H field to the leading order. In fact, ω_n and ψ_n were identified as the frequency and mode structure, respectively, of the TM_{0n} waveguide mode for circular geometry in particular. The first index 0 is the only choice that assures of nonzero resonance strength β_n, or equivalently, nonzero magnetic-dipole moment. Accordingly, $\omega_n=x_{0n}c/r\sqrt{\varepsilon_d}$ and $\psi_n=J_0(x_{0n}\rho/r)$, where x_{0n} is the nth zero of $J_0(x)$ and ρ is the radial coordinate with the origin at the cylinder center.[18] It follows that $\langle\psi_n,1\rangle=2\pi r^2 J_1(x_{0n})/x_{0n}$, $\langle\psi_n,\psi_n\rangle=\pi r^2 J_1^2(x_{0n})$, $\langle 1,1\rangle=\pi r^2$, and therefore $\beta_n=4/x_{0n}^2$.[19] Near the lowest resonance frequency ω_1, Eq. (3) is approximated as

$$\mu_{\text{eff}}\approx 1-\frac{f\beta_1\omega^2}{\omega^2-\omega_1^2}, \tag{4}$$

where the resonance strength $\beta_1=0.692$ $(x_{01}\approx 2.405)$ is a constant. For other geometries, β_1 is slightly different; for example, $\beta_1=64/\pi^4\approx 0.657$ for square shape.

III. RESULTS AND DISCUSSION

A. Magnetism in photonic crystals

Figure 1(a) shows the dispersion diagram for a periodic array of dielectric circular cylinders of radius $r/a=0.2$ and dielectric constant $\varepsilon_d=55$. A typical dispersion pattern with strong resonance is observed between the first two frequency branches for TE polarization. The second branch goes to higher frequencies as the wave vector magnitude increases. This is in contrast to the case of weak resonance where the second branch usually goes to lower frequencies (a typical phenomenon of band folding). In particular, the basic two TE branches experience an *anticrossing* interaction with respect to the light line [cf. the black (inclined) dashed line in Fig. 1(a)] in the range $\Gamma-X$. This phenomenon will occur when the eigenmodes on the two adjacent branches possess the *like symmetry* and the intersection of branches is avoided.[20] The like symmetry is manifest on the H field patterns of the eigenmodes at the lower and upper band edges [the insets of Fig. 1(a)], which belong to the first and second branches, respectively. These patterns depict the localized nature associated with magnetic resonance, where the H fields are largely concentrated within individual dielectric cylinders with rather weak interactions between neighboring cells. This feature also reflects to the fact that a very inhomogeneous field distribution is required to produce a strong magnetic activity.[1]

The lowest Lorentz-type oscillator frequency is obtained by solving the corresponding eigensystem, $-\nabla^2\psi=\varepsilon_d(\omega/c)^2\psi$, to give $\omega_1=0.254(2\pi c/a)$. This frequency is almost identical to that at the lower band edge [cf. the red (horizontal) dashed line in Fig. 1(a)]. Based on Eq. (4), the effective permeability μ_{eff} in terms of the Lorentz-type oscillator is plotted in Fig. 1(b). At the oscillator resonance ω_1, μ_{eff} diverges and the region of negative μ_{eff} coincides well with the forbidden gap in the dispersion diagram. The field pattern of ψ_1 is shown in Fig. 1(c) and the corresponding resonance strength is calculated to give $\beta_1=0.703$ [cf. Eq. (3)], which is close to the ideal value of 0.692 for circular geometry. Note that ω_1 is also close to the TM_{01} waveguide mode frequency for the same radius and dielectric constant $x_{01}c/r\sqrt{\varepsilon_d}=0.258(2\pi c/a)$. Near the resonance, the polariza-

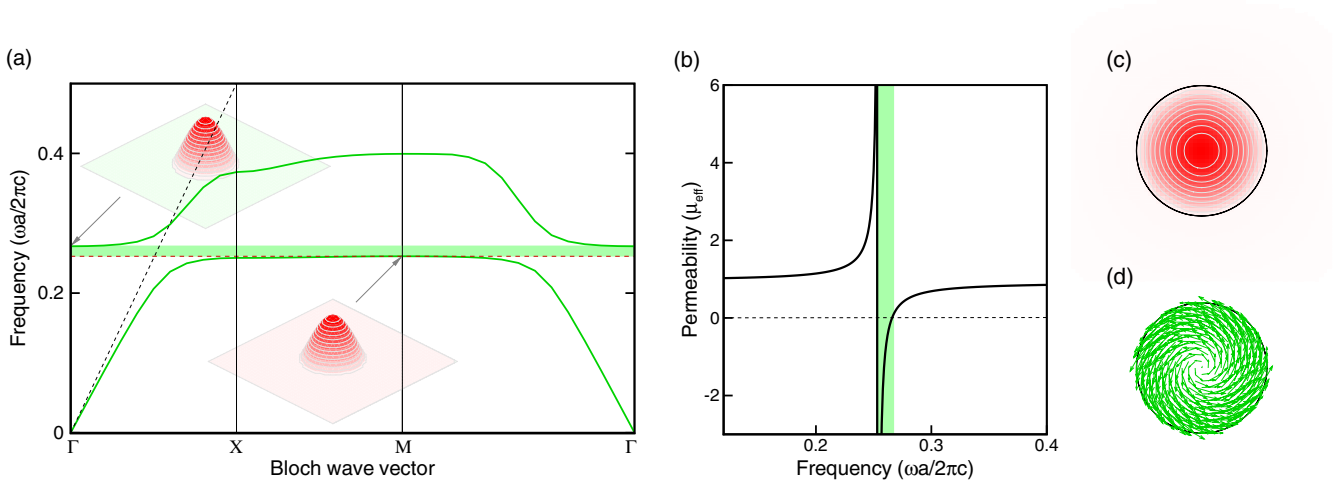

FIG. 1. (Color online) (a) Dispersion diagram for a periodic array of dielectric circular columns with radius $r/a=0.2$ and dielectric constant $\varepsilon_d=55$. Shaded area corresponds to the forbidden gap. Black (inclined) dashed line stands for the light line and red (horizontal) dashed line denotes the lowest Lorentz-type oscillator frequency ω_1. Insets show the eigenmodes at the upper and lower band edges. (b) Effective permeability μ_{eff} based on Eq. (4). (c) Field contours of the eigenfunction ψ_1 in Eq. (3). (d) Polarization current vectors $\mathbf{J}_p$ associated with ψ_1.

tion currents $\mathbf{J_p} \equiv \partial \mathbf{P}/\partial \mathbf{t}$ are circulating around the dielectric column as shown in Fig. 1(d), which give rise to a substantial magnetic-dipole moment along the column axis.

B. Magnetism in split-ring structures

Similar dispersion characteristics and artificial magnetism stated in Sec. III A occur in split-ring structures as well. Figure 2(a) shows the dispersion diagram for a periodic array of split-ring columns with the internal radius $r_i/a=0.2$ being the same as the cylinder radius of the photonic crystal in Fig. 1. The skin depth of the metal is assumed to be vanishingly small. Both the ring thickness $t/a=0.04$ and the gap distance $d/a=0.04$ are small enough in order to give a better correspondence with the photonic structure. First, the dispersion diagram displays a similar resonance pattern (at about the same frequency range) as the photonic structure in Fig. 1. The anticrossing interaction (with respect to the light line) occurs between the first two TE branches and is realized by the like symmetry of eigenmodes at the upper and lower band edges [cf. the insets of Fig. 2(a)]. A minor distinction is that the second branch goes to relatively higher frequencies (than those in the photonic crystal) at the symmetric points X and M.

Compared to photonic crystals, the split-ring structure exhibits a more efficient mechanism of magnetic resonance. As shown in the insets of Fig. 2(a), the H fields of the eigenmodes at the two band edges are nearly constant inside the split ring. This is in contrast with the outward decaying pattern (Bessel function) for the dielectric structure [cf. the in-

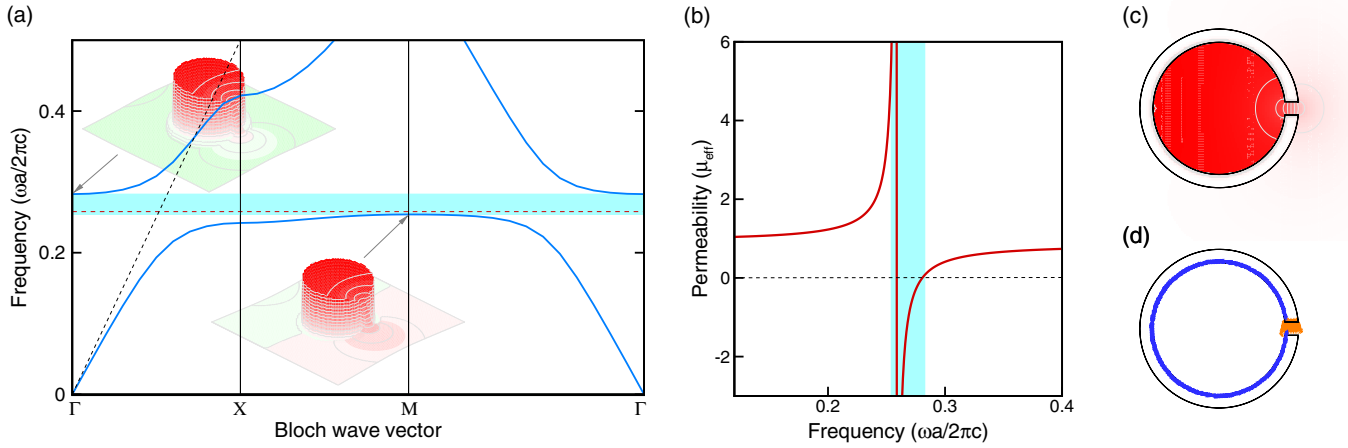

FIG. 2. (Color online) (a) Dispersion diagram for a periodic array of circular split-ring columns with inner radius $r_i/a=0.2$, ring thickness $t/a=0.04$, and gap distance $d/a=0.04$. Insets show the eigenmodes at the upper and lower band edges. (b) Effective permeability μ_{eff} based on Eq. (4). (c) Field contours of the eigenfunction ψ_1 in Eq. (3). (d) Polarization current vectors $\mathbf{J}_p$ (in the ring) and displacement current vectors $\mathbf{J}_d$ (in the gap) associated with ψ_1.

sets of Fig. 1(a)]. Based on the theory of mesoscopic magnetism,[8] the internal fraction of split ring takes the place of high dielectric region and Eq. (3) can be utilized to express the effective permeability with a slight modification to the equation and boundary condition for ψ. The respective eigensystem is modified as $-\nabla^2\psi=(\omega/c)^2\psi$, defined over the unit cell with ψ satisfying the radiation boundary condition at the boundary.[21] Accordingly, the lowest Lorentz-type oscillator frequency for the present configuration is solved to give $\omega_1=0.258(2\pi c/a)$. This frequency is sufficiently close to the lower band edge [cf. the red (horizontal) dashed line in Fig. 2(a)], although there is a small discrepancy in between. Based on Eq. (4), the effective permeability μ_{eff} in terms of the Lorentz-type oscillator is plotted in Fig. 2(b), which has a close resemblance to that for the photonic crystal [cf. Fig. 1(b)]. The field pattern of eigenfunction ψ_1 is plotted in Fig. 2(c), and the corresponding resonance strength is calculated to give $\beta_1=1.217$. This value is substantially larger than that in the photonic crystal ($\beta_1=0.703$), which confirms that the resonance mechanism is more efficient and the split-ring structures act like arrays of high-Q cavities. The region of negative μ_{eff} basically coincides with the forbidden gap in the dispersion diagram, though not as good as the case of photonic crystal. Near the resonance, the polarization currents $\mathbf{J_p}$ are circulating around the ring element, as shown in Fig. 2(d). In the gap region, the displacement currents $\mathbf{J}_d \equiv \varepsilon_0 \partial \mathbf{E}/\partial t$ fill the disconnected portion of polarization currents to build a close current loop. This produces a magnetic-dipole moment similar to that in the photonic crystal [cf. Fig. 1(d)].

Anticipating an ideal condition where both the ring thickness and gap distance are vanishingly small, ψ_1 may approach a constant inside the split ring and exactly null outside, and therefore $\beta_1 \approx \langle 1,1\rangle^2/\langle 1,1\rangle^2=1$ [cf. Eq. (3)]. This result corresponds to the effective-medium theory based on the equivalent circuit model $\mu_{\text{eff}}=1-f\omega^2/(\omega^2-\omega_0^2)$,[1] where the intrinsic LC resonance frequency ω_0 plays the same role of the lowest Lorentz-type oscillator frequency ω_1. For a real split-ring configuration, ψ_1 could be slightly deformed around the ring gap, causing β_1 to deviate from unity to a certain extent.

C. Anticrossing interaction

Anticrossing interaction between the two fundamental branches in the dispersion diagram appears as another distinguished feature of resonance associated with artificial magnetism. This phenomenon occurs when the mode structures on two adjacent frequency branches possess the *like symmetry*; the intersection of branches is thus avoided.[22] In the present study, the anticrossing behavior is manifest on the photonic crystal with large dielectric contrast, as well as on the split-ring structure with sufficient internal fraction.

To demonstrate the dependence of anticrossing behavior on the dielectric contrast, Fig. 3(a) shows the frequency branches for the photonic crystal with $r/a=0.2$ for various ε_d. The frequency has been scaled with $2\pi c/r\sqrt{\varepsilon_d}$ (instead of $2\pi c/a$) in order to identify the anticrossing phenomenon at about the same range. In the present configuration, the anti-

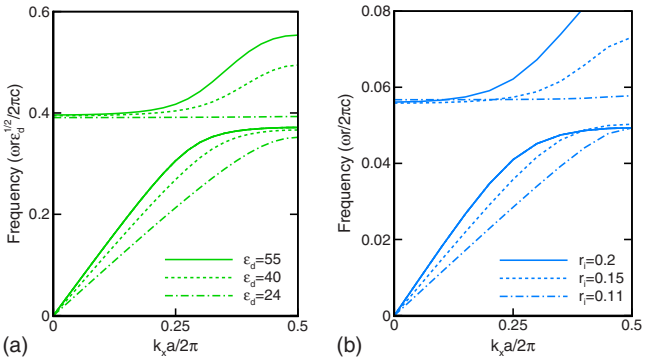

FIG. 3. (Color online) Anticrossing phenomenon in (a) photonic crystals with $r/a=0.2$ for various dielectric contrasts, and (b) split-ring structures with $t/a=0.01$ and $d/a=0.01$ for various internal radius r_i.

crossing scheme arises when the dielectric contrast exceeds a threshold value ($\varepsilon_d \approx 24$), at which the second branch appears as a flat band in the range $\Gamma-X$. As the dielectric contrast is further increased, the anticrossing pattern becomes more evident. Below the threshold, the second branch behaves as an ordinary optical branch in most periodic structures; that is, the branch goes downward as the wave vector magnitude increases.

A similar feature appears in the split-ring structures for various internal radius r_i/a, as shown in Fig. 3(b). Both the ring thickness and gap distance are kept at small values. Likewise, the frequency is scaled with $2\pi c/r$ (instead of $2\pi c/a$) to identify the anticrossing behavior at about the same range. The anticrossing scheme is more evident for larger internal fractions. Below the threshold ($r_i/a \approx 0.11$), where the second branch becomes flattened, the anticrossing behavior no longer exists. As in the case of photonic crystal, the upper bound of the first branch as well as the lower bound of the second is approximately located at the same positions. The band gap opens as the anticrossing appears, and artificial magnetism becomes a significant feature.

The anticrossing behavior has been studied for the optical properties of metallodielectric photonic crystals.[23] In conjunction with the effective-medium description and group-theory analysis, the hybridization of states in two bands gives rise to an induced frequency gap. The anticrossing interaction usually occurs between a heavy and a light photon band;[24] the former is referred to a strong localized photon state and the latter to a nearly free photon state.[25] In photonic crystals, the localization feature can be achieved by increasing the dielectric contrast, while the localization in split-ring structures is attained by introducing a gap (into the ring) to form a defectlike state.[26] Both situations correspond to a heavy photon state, along with it comes a dispersionless or flattened band. Once there is a coupling between the two states, the respective branches tend to repel each other.[27] This feature can be characterized by a simple dynamic model analogous to that in the analysis of electronic energy bands in solids[28] and semiconductor alloys.[29] Denoting by α the coupling coefficient between a free photon state H_0 (with frequency ck) and a localized photon state H_1 (with the lowest Lorentz-type oscillator frequency ω_1), one has

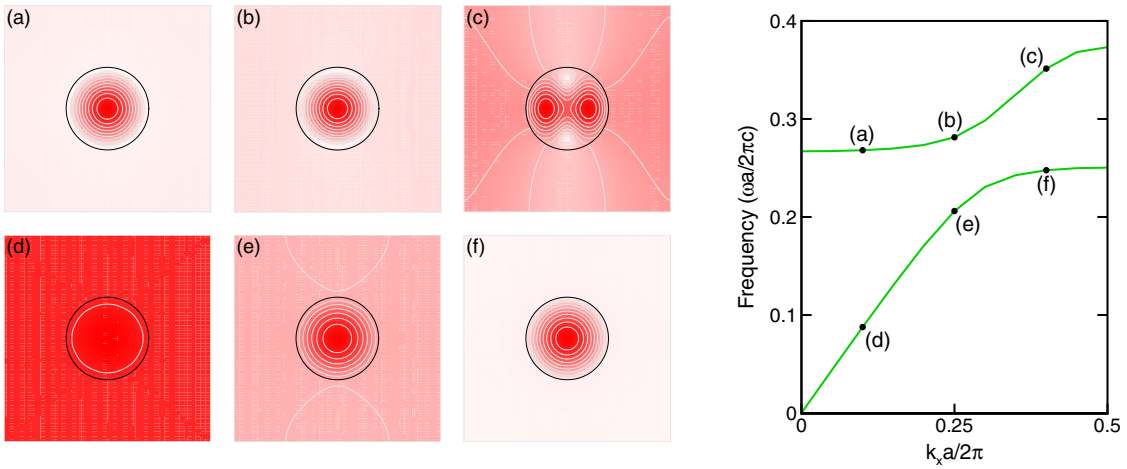

FIG. 4. (Color online) Transition of mode patterns for the photonic crystal in Fig. 1 on the upper branch with (a) $k_x a/2\pi=0.1$, (b) 0.25, and (c) 0.4 and on the lower branch with (d) $k_x a/2\pi=0.1$, (e) 0.25, and (f) 0.4. The color intensity denotes the magnitude of magnetic field. Respective locations of the modes (a)–(f) are marked in the right plot.

$$\ddot{H}_0 + c^2k^2H_0 = \alpha H_1, \tag{5}$$

$$\ddot{H}_1 + \omega_1^2 H_1 = \alpha H_0. \tag{6}$$

The above equations lead to the condition of nontrivial solution as

$$\begin{vmatrix} \omega^2 - c^2k^2 & \alpha \\ \alpha & \omega^2 - \omega_1^2 \end{vmatrix} = 0, \tag{7}$$

and the two solutions are given by

$$\omega_\pm^2 = \frac{1}{2}[\omega_1^2 + c^2k^2 \pm \sqrt{(\omega_1^2 - c^2k^2)^2 + 4\alpha^2}]. \tag{8}$$

In this approximate model, the coupling constant α is a measure of the interaction strength. The repelling of the two states (from the presumed crossing point) is characterized by 2α; the high-frequency state shifts by $+\alpha$, while the low-frequency state shifts by $-\alpha$. In addition, as the photon states gain momentum (by increasing k), their characteristics are mutually exchanged: ω_- changing from ck to ω_1, while ω_+ changing from ω_1 to ck.

The change of frequency is accompanied with the transition of mode pattern. For illustration, the transition of mode patterns on the two interaction branches is plotted in Fig. 4 for the same photonic crystal in Fig. 1. As the wave number increases, the modes on the upper branch [Figs. 4(a)–4(c)] gradually lose their localized nature; the fields are no longer concentrated within the dielectric region only. On the other hand, the modes on the lower branch [Figs. 4(e) and 4(f)] change in the opposite manner; the fields gain localization with increasing the wave number. Similar mode transitions for the split-ring structure are illustrated in Fig. 5. The trend of losing or gaining localization on the respective branch is alike, and the repelling between the branches are more evident, which is attributable to a larger interaction strength (or the coupling constant α) for the split-ring structure. This consists with the nearly optimal resonance strength β_1 asso-

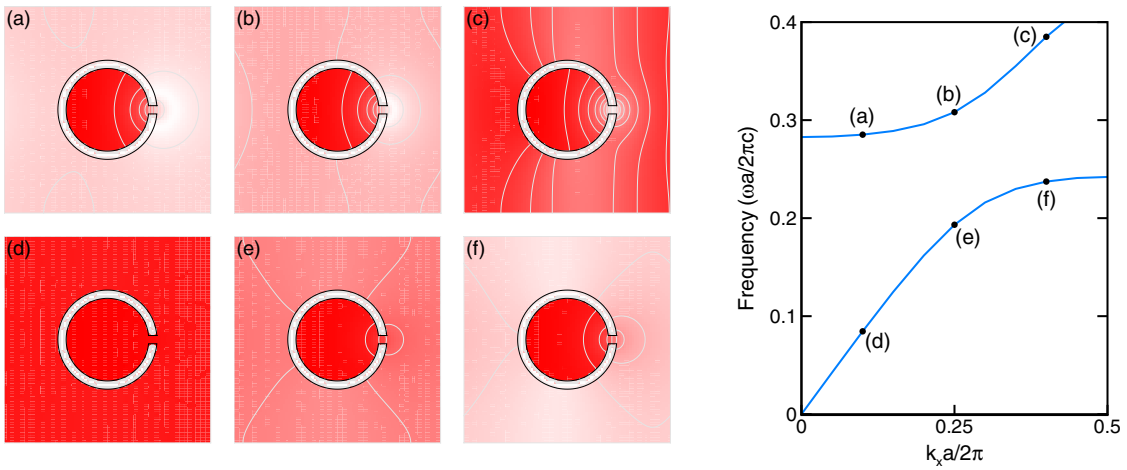

FIG. 5. (Color online) Transition of mode patterns for the split-ring structure in Fig. 2 on the upper branch with (a) $k_x a/2\pi=0.1$, (b) 0.25, and (c) 0.4 and on the lower branch with (d) $k_x a/2\pi=0.1$, (e) 0.25, and (f) 0.4. The color intensity denotes the magnitude of magnetic field. Respective locations of the modes (a)–(f) are marked in the right plot.

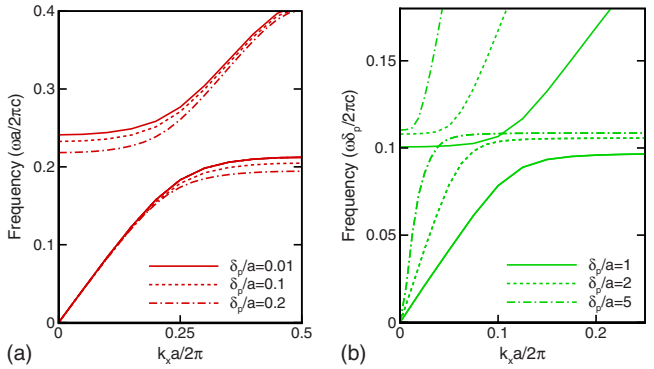

FIG. 6. (Color online) Effect of skin depth on the dispersion characteristics for the split-ring structure in Fig. 2. (a) $\delta_p/a<1$, (b) $\delta_p/a\geq 1$.

ciated with the split-ring element. A similar transition behavior is also observed between the defectlike and corelike modes in the fiber structure.[30]

Finally, the effect of skin depth on artificial magnetism and anticrossing interaction for the split-ring structure is shown in Fig. 6 by applying the free-electron model $\varepsilon=1-\omega_p^2/\omega^2$ for the dielectric function, where ω_p is the bulk plasma frequency of the metal. The skin depth is defined as $\delta_p\equiv 2\pi c/\omega_p$. For relatively small skin depths ($\delta_p/a<1$) in Fig. 6(a), the dispersion features slightly deviate from the case of $\delta_p\approx 0$; the frequency branches tend to level down as δ_p/a increases. The anticrossing interaction and resonance band gap due to artificial magnetism is still present. For relatively large skin depths ($\delta_p/a\geq 1$) in Fig. 6(b), the dispersion characteristics alter in two aspects. First, the branches drop to much lower frequencies and it is more adequate to scale the frequency with $2\pi c/\delta_p$ (instead of $2\pi c/a$). This feature amounts to the saturation of magnetic resonance with respect to the structure size and is attributed to the *kinetic inductance* caused by the increasing importance of kinetic energy of free electrons.[31,32] Second, the resonance region gradually shrinks to a rather small band width and the anticrossing behavior becomes less significant. As the skin depth is further increased, the frequency branches apparently bend toward $k_x=0$; the lower branch grows into a flat band at a smaller wave number and the higher branch rises abruptly to a much higher frequency.

IV. CONCLUDING REMARKS

In conclusion, artificial magnetism and anticrossing interaction in photonic crystals and split-ring structures were investigated. Near the resonance, the two types of structures exhibit similar dispersion features, along with highly localized eigenmode patterns. The correspondence is more evident when the dielectric contrast of the photonic crystal becomes larger and both the ring thickness and gap distance of the split-ring structure become smaller. The effective permeabilities for both structures are well described in terms of the Lorentz-type oscillators based on the theory of mesoscopic magnetism.[8] Compared to photonic crystals, the split-ring structures show a more efficient and nearly optimal resonance mechanism and act like arrays of high-Q cavities. This situation corresponds with the equivalent circuit model,[1] in which the intrinsic LC resonance serves as the lowest Lorentz-type oscillator. Strong magnetic response is also accompanied with the anticrossing interaction between the two fundamental frequency branches, which was manifest on the like symmetry of eigenmodes at the two band edges. The respective frequency branches repel each other, showing the coupling between a free photon state and a localized photon state. This anticrossing behavior was characterized by a simple dynamic model which incorporates the coupling coefficient between the two states as the interaction strength and illustrated with the transition of mode patterns where the fields mutually exchange their localization nature as the wave number changes.

ACKNOWLEDGMENTS

This work was supported in part by National Science Council of the Republic of China under Contracts No. NSC 96-2221-E-002-190-MY3 and No. NSC 97-2120-M-002-013.

*chern@iam.ntu.edu.tw

[1] J. B. Pendry, A. J. Holden, D. J. Robbins, and W. J. Stewart, IEEE Trans. Microwave Theory Tech. **47**, 2075 (1999).
[2] D. R. Smith and N. Kroll, Phys. Rev. Lett. **85**, 2933 (2000).
[3] D. R. Smith, J. B. Pendry, and M. C. K. Wiltshire, Science **305**, 788 (2004).
[4] T. J. Yen, W. J. Padilla, N. Fang, D. C. Vier, D. R. Smith, J. B. Pendry, D. N. Basov, and X. Zhang, Science **303**, 1494 (2004).
[5] S. Linden, C. Enkrich, M. Wegener, J. Zhou, T. Koschny, and C. Soukoulis, Science **306**, 1351 (2004).
[6] J. D. Baena, L. Jelinek, R. Marques, and M. Silveirinha, Phys. Rev. A **78**, 013842 (2008).
[7] S. O'Brien and J. B. Pendry, J. Phys.: Condens. Matter **14**, 4035 (2002).
[8] D. Felbacq and G. Bouchitté, Phys. Rev. Lett. **94**, 183902 (2005).
[9] C. Rockstuhl, U. Peschel, and F. Lederer, J. Opt. Soc. Am. A Opt. Image Sci. Vis. **24**, A60 (2007).
[10] C. Tserkezis, N. Papanikolaou, G. Gantzounis, and N. Stefanou, Phys. Rev. B **78**, 165114 (2008).
[11] R. L. Chern, C. C. Chang, C. C. Chang, and R. R. Hwang, Phys. Rev. E **68**, 026704 (2003).
[12] C. C. Chang, J. Y. Chi, R. L. Chern, C. C. Chang, C. H. Lin, and C. O. Chang, Phys. Rev. B **70**, 075108 (2004).
[13] R. L. Chern, C. C. Chang, and C. C. Chang, Phys. Rev. B **73**, 235123 (2006).
[14] R. L. Chern, C. C. Chang, and C. C. Chang, Phys. Rev. B **74**, 155101 (2006).

[15] R. L. Chern, Phys. Rev. B **77**, 045409 (2008).
[16] D. Felbacq and G. Bouchitté, Opt. Lett. **30**, 1189 (2005).
[17] D. Felbacq and G. Bouchitté, New J. Phys. **7**, 159 (2005).
[18] D. M. Pozar, *Microwave Engineering*, 3rd ed. (Wiley, New York, 2005).
[19] N. A. Mortensen, S. Xiao, and D. Felbacq, J. Eur. Opt. Soc. Rapid Publ. **1**, 06019 (2006).
[20] L. D. Landau and E. M. Lifshitz, *Quantum Mechanics: Non-Relativistic Theory* (Butterworth-Heinemann, Oxford, 1981).
[21] G. Bouchitté and D. Felbacq, C. R. Acad. Sci., Ser. I: Math. **339**, 377 (2004).
[22] L. D. Landau, E. M. Lifshitz, and L. P. Pitaevskii, *Electrodynamics of Continuous Media*, 2nd ed. (Butterworth-Heinenann, Oxford, 1984).
[23] V. Yannopapas, A. Modinos, and N. Stefanou, Phys. Rev. B **60**, 5359 (1999).
[24] S. Yano, Y. Segawa, J. S. Bae, K. Mizuno, S. Yamaguchi, and K. Ohtaka, Phys. Rev. B **66**, 075119 (2002).
[25] E. Lidorikis, M. M. Sigalas, E. N. Economou, and C. M. Soukoulis, Phys. Rev. B **61**, 13458 (2000).
[26] A. B. Movchan and S. Guenneau, Phys. Rev. B **70**, 125116 (2004).
[27] S. Mahnkopf, M. Kamp, A. Forchel, F. Lelarge, G. H. Duan, and R. März, Opt. Commun. **239**, 187 (2004).
[28] W. A. Harrison, *Solid State Theory* (Dover, New York, 1979).
[29] W. Shan, W. Walukiewicz, J. W. Ager III, E. E. Haller, J. F. Geisz, D. J. Friedman, J. M. Olson, and S. R. Kurtz, Phys. Rev. Lett. **82**, 1221 (1999).
[30] T. Engeness, M. Ibanescu, S. Johnson, O. Weisberg, M. Skorobogatiy, S. Jacobs, and Y. Fink, Opt. Express **11**, 1175 (2003).
[31] J. Zhou, T. Koschny, M. Kafesaki, E. N. Economou, J. B. Pendry, and C. M. Soukoulis, Phys. Rev. Lett. **95**, 223902 (2005).
[32] M. W. Klein, C. Enkrich, M. Wegener, C. M. Soukoulis, and S. Linden, Opt. Lett. **31**, 1259 (2006).